doi:10.1016/j.jmb.2008.05.087 J. Mol. Biol. (2008) 381, 361–372

JMB

Available online at www.sciencedirect.com

ScienceDirect

ELSEVIER

Structure of a Second BRCT Domain Identified in the Nijmegen Breakage Syndrome Protein Nbs1 and its Function in an MDC1-Dependent Localization of Nbs1 to DNA Damage Sites

Chao Xu[1], Liming Wu[2], Gaofeng Cui[1], Maria Victoria Botuyan[1], Junjie Chen[2] and Georges Mer[1]*

[1]*Department of Biochemistry and Molecular Biology, Mayo Clinic College of Medicine, Rochester, MN 55905, USA*

[2]*Department of Therapeutic Radiology, Yale University School of Medicine, New Haven, CT 06520, USA*

Received 18 April 2008; accepted 27 May 2008
Available online
14 June 2008

The Nijmegen breakage syndrome protein Nbs1 is a component of the MRN (Mre11–Rad50–Nbs1) complex, central to the DNA damage response. While Nbs1 is generally believed to encompass a forkhead-associated domain linked to a breast cancer C-terminal (BRCT) domain, to date there is no experimental information on its three-dimensional structure. Through nuclear magnetic resonance (NMR) three-dimensional structure determination, we demonstrate that there is a second BRCT domain (BRCT2) in Nbs1. The domain has the characteristic BRCT topology, but with a long insertion shown to be flexible by NMR relaxation measurements. In the absence of sequence similarity to other proteins, a search for structural analogs of BRCT2 returned the second BRCT domain of the tandem BRCT repeats of cell cycle checkpoint proteins MDC1 (mediator of DNA damage checkpoint protein 1) and BRCA1 (breast cancer protein 1), suggesting that like MDC1 and BRCA1, Nbs1 also possesses tandem BRCT domains with phosphoprotein binding ability. Structure-based single point mutations in human Nbs1 were evaluated *in vivo* and revealed that BRCT2 is essential for an MDC1-dependent relocalization of Nbs1 to DNA damage sites, most likely through a direct interaction of Nbs1 tandem BRCT domains with phosphorylated MDC1.

Keywords: Nijemegen breakage syndrome; Nbs1; MDC1; DNA damage response; BRCT domain

Edited by M. F. Summers

Introduction

The Nijmegen breakage syndrome (NBS) is a genetic disorder characterized by severe microcephaly, growth retardation, immunodeficiency, and predisposition to cancer, particularly lymphomas.[1,2] Cells from patients with NBS show hypersensitivity to ionizing radiation (IR), chromosomal instability, and abnormal p53-mediated cell cycle regulation.[3–7] NBS results from mutations in the *NBS1* gene[8,9] whose normal protein product, the 754-amino-acid protein Nbs1 (also called nibrin or p95), associates with Mre11 and Rad50 to form the MRN (Mre11–Rad50–Nbs1) complex.[10,11] MRN is known to play a key role in sensing DNA strand breaks and then amplifying initial signal and transducing it to downstream effector proteins that regulate cell cycle checkpoint and DNA repair.[12–15] In the MRN complex, Nbs1 regulates the catalytic nucleotide-dependent DNA binding and ATP-dependent DNA unwinding functions of Mre11 and Rad50.[16,17] It is also required for the localization of Mre11 and Rad50 into the nucleus as well as for the activation of ataxia–telangiectasia mutated (ATM) kinase.[18–21] The majority of patients with NBS have the 657del5 mutation in exon 6 of *NBS1*, which splits the Nbs1 protein into a 26-kDa

**Corresponding author.* E-mail address: mer.georges@mayo.edu.

Abbreviations used: BRCT, breast cancer C-terminal; NBS, Nijmegen breakage syndrome; Nbs1, Nijmegen breakage syndrome protein; IR, ionizing radiation; MRN, Mre11–Rad50–Nbs1; ATM, ataxia–telangiectasia mutated; BRCA1, breast cancer protein 1; MDC1, mediator of DNA damage checkpoint protein 1; XNbs1, *Xenopus laevis* Nbs1; HSQC, heteronuclear single-quantum coherence; NOE, nuclear Overhauser enhancements; CK2, casein kinase 2.

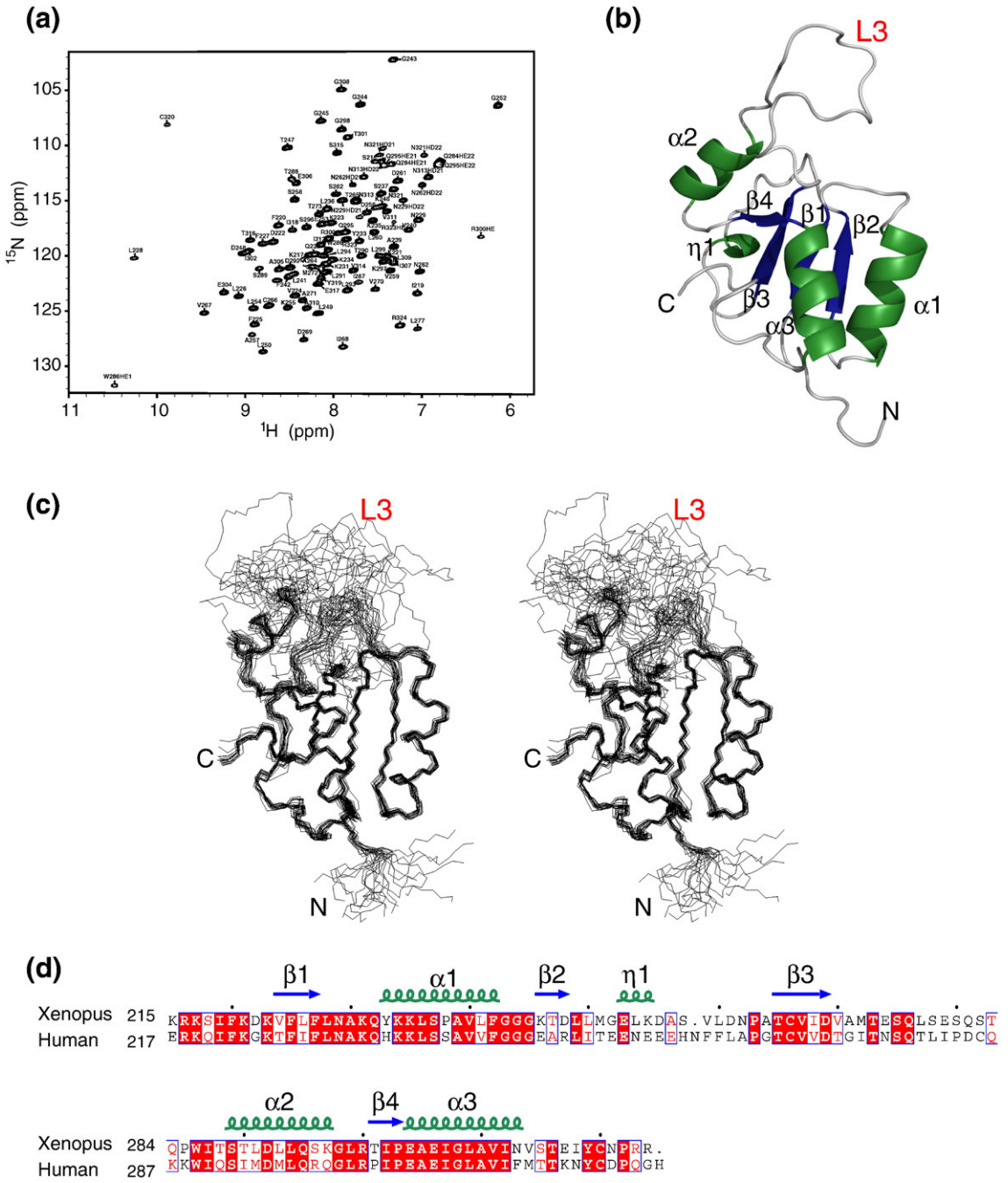

Fig. 1. Solution NMR structure of XNbs1 (residues 215 to 324). (a) ^{1}H–^{15}N HSQC spectrum of XNbs1 with labeled signals. (b) Ribbon representation of XNbs1 BRCT2. The secondary-structure elements are indicated. The disordered loop L3 is shown in red. (c) Stereo view of the superimposed 20 lowest-energy structures. The disordered loop L3 is shown in red. (d) Amino acid sequence alignment of *X. laevis* and human Nbs1. The secondary-structure elements of XNbs1 are shown above the sequences. η1 is a short helical turn. The alignment was created with ESPript (http://espript.ibcp.fr/ESPript/ESPript/).

(p26, 1–218 amino acids or aa) and a 70-kDa (p70, 221–754 aa) proteins.[8,9,22] p26 is unable to form the MRN complex. p70 still binds Mre11 and Rad50 but is defective in a number of functions including nuclear focus formation and intra-S and G_2/M phase checkpoint response.

No structural information is currently available for Nbs1. Much of what is known about the structural domains of Nbs1 comes from limited sequence alignment with other proteins. The N-terminal region of human Nbs1 contains a forkhead-associated (FHA) domain (24–108 aa)[23] and a breast cancer C-terminal (BRCT) domain (108–196 aa).[24,25] The FHA domain is a common motif involved in phosphothreonine or phosphoserine recognition in many proteins,[26] while two BRCT domains in tandem can form a phosphopeptide binding motif as shown for breast cancer protein 1 (BRCA1) and mediator of DNA damage

checkpoint protein 1 (MDC1).[27–34] The C-terminal region of Nbs1 contains the Mre11-binding site as well as the ATM-binding site.[35,36] In response to induction of DNA double-strand breaks, human Nbs1 is phosphorylated at four serine residues by ATM kinase.[37–39] Efficient phosphorylation is achieved when Nbs1 is maintained in a hypoacetylated state by the SIRT1 deacetylase.[40] So far, two acetylation sites, Lys233 and Lys690, have been identified in Nbs1.

In this study, by means of nuclear magnetic resonance (NMR) spectroscopy structure determination, we have identified a second BRCT domain (BRCT2) downstream from BRCT1 in *Xenopus laevis* Nbs1 (XNbs1) in a region of the protein that has no significant amino acid sequence homology to other BRCT domains, thus confirming a recent prediction.[41] BRCT2, which is conserved in human Nbs1, has the familiar α/β topology characteristic of BRCT domains in other proteins but differs markedly in having a disordered long loop inserted between a β strand and an α helix, as determined by NMR relaxation measurements. This corresponding loop in human Nbs1 has one of the serine residues phosphorylated by ATM kinase. Nbs1 BRCT2 also contains one of the two acetylation sites regulated by SIRT1. Structure comparison to MDC1 and BRCA1 tandem BRCT domains suggests that BRCT2 and BRCT1 of Nbs1 form a tandem repeat that could recognize a phosphorylated protein target. Through structure-directed mutagenesis, we show that *in vivo* BRCT2 is essential for an MDC1-facilitated nuclear relocalization of Nbs1 to DNA damage sites, and our data suggest a direct interaction between Nbs1 tandem BRCT domains and phosphorylated MDC1.

Results and Discussion

Identification of a second BRCT domain (BRCT2) in Nbs1

A 110-amino-acid fragment (215–324 aa) of XNbs1 was chosen for our structural studies based on an initial PONDR analysis of its amino acid sequence (data not shown).[42] The program, which predicts regions of disorder from a given amino acid sequence, predicted the central region up to the C-terminus of XNbs1 (322–763 aa) and human Nbs1 (328–754 aa) to be mainly disordered. In contrast, the N-terminal regions of these proteins are predicted by PONDR to be mainly folded. In human Nbs1, the ordered region contains the FHA domain (24–108 aa) and the BRCT domain (108–196 aa). It also includes a stretch of 110 amino acids (218–327 aa), which does not show any marked sequence similarity with other known structural domains. It was, however, proposed that a similar fragment could adopt a BRCT fold based on hidden Markov modeling profiling and structure modeling results.[41]

We initiated structural studies on the 217–330 aa fragment of human Nbs1. While this segment of the protein is folded as verified by NMR spectroscopy (data not shown), its poor expression in *Escherichia coli* prompted us to use the corresponding region from *X. laevis*, which is homologous to the human sequence (47% amino acid sequence identity) and is well expressed in *E. coli*. The nice dispersion of peaks in the ^{1}H–^{15}N heteronuclear single-quantum coherence (HSQC) spectrum of XNbs1 (215–324 aa), an indication of a folded structure, is shown in Fig. 1a. We have determined the three-dimensional (3-D) structure of this XNbs1 fragment by triple-resonance heteronuclear NMR spectroscopy. A ribbon representation of the molecule and the superimposed structures from a family of 20 are shown in Fig. 1b and c. The structures, which span from residues Lys215 to Arg324, are well converged with average pairwise root-mean-square deviations (r.m.s.d.s) of 0.78 and 1.39 Å over backbone and all heavy atoms, respectively, but excluding flexible regions (Table 1). There are eight residues (MHHHHHHM) that include a hexahistidine purification tag prior to the actual XNbs1 sequence. From this N-terminal sequence, only the last methionine was included with the XNbs1 sequence in the structure calculation protocols. A PROCHECK[43] evaluation of the final 20 structures indicates that ~99% of the residues lie in the most favored and additionally allowed regions of the Ramachandran plot (Table 1).

Table 1. NMR and refinement statistics for XNbs1 BRCT2 structure

NMR distance and dihedral angle constraints	
Distance constraints	
Total NOE	2286
Intraresidue	316
Interresidue	1970
Sequential ($\|i-j\|=1$)	592
Medium range ($\|i-j\|<4$)	564
Long range ($\|i-j\|>5$)	814
Hydrogen bonds	32
Total dihedral angle restraints	
ϕ	52
ψ	52
Structure statistics	
Violations (mean±standard deviation)	
No. of distance constraints >0.2 Å	3.2±0.8
No. of dihedral angle constraints >3.0°	4.3±1.7
Maximum dihedral angle violation (°)	3.0±1.5
Maximum distance constraint violation (Å)	0.19±0.04
Deviations from idealized geometry	
Bond lengths (Å)	0.008
Bond angles (°)	1.8
Impropers (°)	3.5
Average pairwise r.m.s.d. (Å)[a]	
Heavy (residues 218–270 and 289–324)	1.39±0.17
Backbone (residues 218–270 and 289–324)	0.78±0.13
Ramachandran space (%)[b]	
Most favored regions	76.4±3.4
Additionally allowed regions	22.8±2.3
Generously allowed regions	0.5±0.3
Disallowed regions	0.8±0.2

The AMBER energy of the 20 refined structures was −5893.86± 23 kcal mol^{-1}.

[a] Pairwise r.m.s.d. was calculated from 20 refined structures.

[b] Ramachandran statistics were calculated with all amino acids, including those in loop L3.

XNbs1 contains a four-stranded parallel β sheet surrounded by three α helices: β1 (224–227 aa), β2 (246–248 aa), β3 (265–269 aa), and β4 (301–303 aa); α1 (233–242 aa), α2 (289–298 aa), and α3 (304–313 aa) (Fig. 1b and d). Based on the overall placement and packing of the secondary-structure elements, our data demonstrate that a BRCT domain (BRCT2) is present within the 215 to 324 aa fragment of XNbs1, therefore confirming the prediction of Becker *et al.*[41] From the high level of sequence homology and location of secondary-structure elements (Fig. 1d), it is clear that this BRCT fold is conserved in human Nbs1. In particular, residues Ile219, Phe220, Phe225, Phe227, Val240, Val268, Ile302, Ile307, Val311, and Cys320 that make up the hydropohobic core of XNbs1 are all strictly conserved in human Nbs1. In addition, another hydrophobic pocket in XNbs1, composed of Leu226, Leu228, Val259, Leu260, Val267, Leu291, and Leu294, is also conserved with identical or homologous residues in human Nbs1. Noticeably, the majority of patients with NBS have a deletion mutation of *NBS1*, which splits the Nbs1 protein at the beginning of BRCT2, giving rise to the p26 (1–218 aa) and p70 (221–754 aa) proteins.[8,9,22]

While the secondary-structure elements of XNbs1 are similar to other known BRCT domains, we also notice a significant difference. Unlike the typical BRCT motif, there is a long insertion in XNbs1. This 18-residue loop, L3, runs from Ala271 to Thr288 and bridges β3 and α2. In contrast, the corresponding loop in human MDC1 BRCT2, the structure with closest similarity to Nbs1 (*vide infra*), is only 4 residues long. The loop L3 is poorly defined in the ensemble of NMR structures (Fig. 1c) due to the very limited number of nuclear Overhauser enhancements (NOEs) in this region.

The phosphorylated loop L3 of Nbs1 BRCT2 is highly flexible

The disordered nature of L3 was confirmed through the calculation of reduced spectral density functions,[44–48] $J(\omega)$, at three frequencies from the backbone ^{15}N-spin relaxation rates R_1 and R_2 and heteronuclear ^{1}H–^{15}N NOEs measured at two magnetic field strengths (600 and 700 MHz, ^{1}H frequency). The spectral density function values $J(0)$, $J(\omega_N)$, and $J(\omega_H+\omega_N)$ for the backbone ^{15}N–^{1}H bond vectors plotted against the amino acid sequence are presented in Fig. 2a and the measured NMR relaxation parameters used to calculate these values are shown in Fig. 2b.

The total surface area under $J(\omega)$ is a constant.[49] How this constant area is distributed is determined by the energy associated with the orientational fluctuations of ^{15}N–^{1}H vectors.[50] Fast internal motions

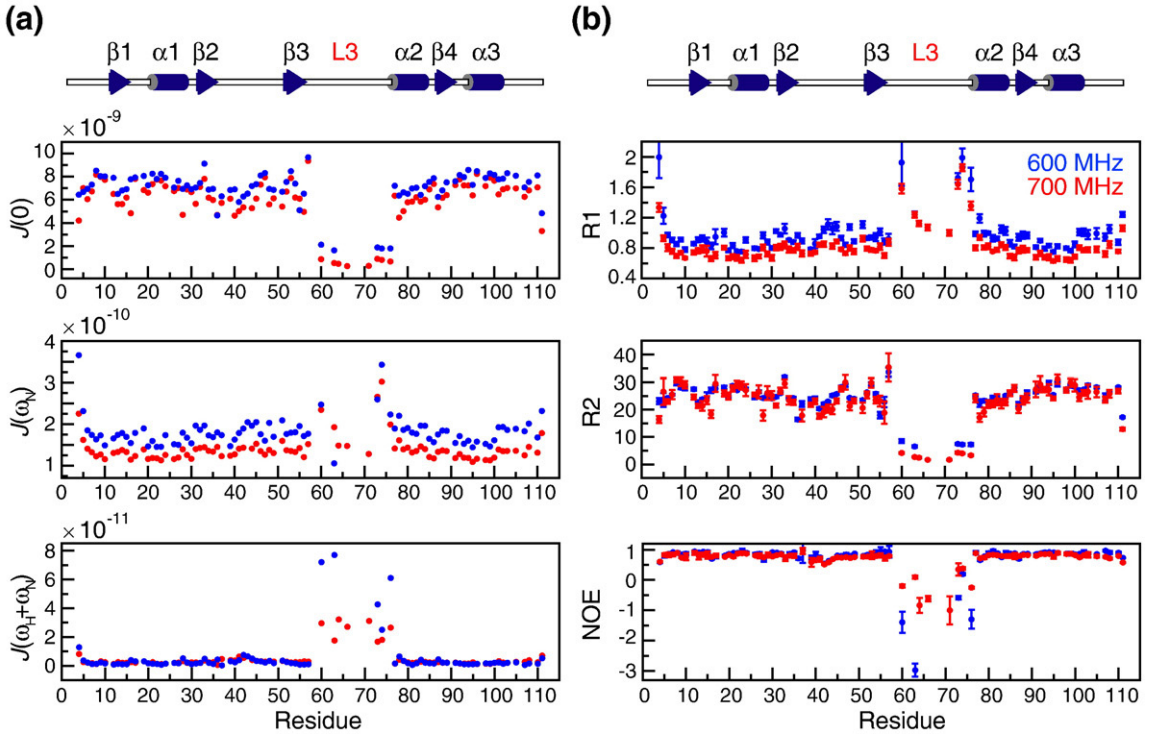

Fig. 2. Structural dynamics of XNbs1 BRCT2. (a) Plot of the spectral density function values (s rad^{-1}) at frequencies 0, ω_N, and $\omega_H+\omega_N$ for XNbs1 BRCT2 as a function of the protein sequence. The blue and red dots are for data recorded at 600 and 700 MHz (^{1}H frequency), respectively. (b) Plot of ^{15}N NMR relaxation rates R_1 (s^{-1}), R_2 (s^{-1}), and ^{1}H–^{15}N NOE as a function of the protein sequence. Experiments were recorded at 600 (blue) and 700 MHz (red), ^{1}H frequency. Uncertainties of the R_1 and R_2 values were evaluated by performing 100 fits with random Gaussian noise added to the experimental intensities. The secondary structure of XNbs1 BRCT2 is indicated at the top of (a) and (b). The actual XNbs1 sequence from 215 to 324 residues has been renumbered from 2 to 111 in this figure.

are expected to increase $J(\omega)$ at higher frequencies and therefore decrease $J(\omega)$ at lower frequencies as a consequence of the conservation of the total $J(\omega)$ area.

The decrease in $J(0)$ values with a corresponding increase in $J(\omega_H+\omega_N)$ observed in L3 is a clear indication of fast motions on time scales of hundreds of picoseconds to several nanoseconds. It is apparent that there are also slow motions on the microsecond to millisecond time scale in L3. This is seen from the increased value of $J(0)$ for Val270 (residue 57 in Fig. 2), and even more so from the observation that several residues in L3 exhibited broadened or even no $^{1}H–^{15}N$ HSQC signals. The relaxation rates and $J(\omega)$ values associated to these broad signals could not be determined and are therefore not shown in Fig. 2. A few other signals were excluded from the analysis because of overlap or lack of resonance assignment. In total, the dynamics of 84 backbone $^{15}N–^{1}H$ vectors could be analyzed at 600 MHz and 87 at 700 MHz.

As is often the case, the very N- and C-terminal residues participate in fast motions on the picosecond to nanosecond time scale as evidenced from the decreased $J(0)$ and increased $J(\omega_N)$ values. The spectral density values outside L3 and N- and C-termini are fairly uniform and correspond to the well-defined secondary-structure elements and connecting loops (Fig. 2a).

It is worth noting that the high level of mobility of loop L3 is evident from the backbone ^{15}N relaxation rates R_1 and R_2 and $^{1}H–^{15}N$ NOEs presented in Fig. 2b, with a dramatic decrease in R_2 and NOEs correlated with a marked increase in R_1, with respect to these parameters in the well-defined regions of the protein. The R_1 and R_2 ^{15}N relaxation rates for residues in the secondary-structure elements of XNbs1 BRCT2 were used to estimate a correlation time (τ_c) of 14±1.0 ns, which is consistent with that of a monomeric species at 15 °C.

There are four sites in human Nbs1 that are phosphorylated by ATM kinase in response to radiation exposure, namely, Ser278, Ser343, Ser397, and Ser615.[37–39,51,52] The counterpart of Ser278 in human Nbs1 is Ser275 in XNbs1 and is contained in the fragment studied here, specifically in the central loop L3. Phosphorylation sites are often located in unfolded regions of proteins. In the case of XNbs1, Ser275 is within a folded BRCT2 domain but in a loop that is highly disordered. The flexible loop may be a docking site for other proteins after (in the case of human Nbs1) phosphorylation of Ser278 by ATM kinase.

One of the three lysine acetylation consensus motifs in human Nbs1, correlated to acetylation of Lys233 by p300/CBP-associated factor or p300 acetyltransferases,[40] is also present in XNbs1 BRCT2 (Lys231) in the loop connecting β1 to α1. Remarkably, Lys231 in our 3-D structure approximately occupies the position of a side chain in MDC1 and BRCA1 that is essential for phosphopeptide binding, suggesting a possible regulatory mechanism of phosphorylation-dependent Nbs1 interaction through acetylation and deacetylation of the human Nbs1 counterpart (Lys233) as explained below.

Structure comparisons suggest that Nbs1 BRCT2 and BRCT1 form a tandem repeat that can recognize a phosphorylated protein target

A search in the Protein Data Bank (PDB) for structural analogs of XNbs1 BRCT2 with the program Dali[53] returned the second BRCT domain of human MDC1 (PDB identification 2ETX:chain B, *Z* score 7.7, r.m.s.d. 2.7 Å with 85 residues, 12% identity) to be the closest match, followed by the second BRCT domain of BRCA1 (PDB identification 1T15:chain A, *Z* score 7.3, r.m.s.d. 3.1 Å with 89 residues, 8% identity). Both MDC1 and BRCA1 have tandem BRCT domains, which strongly suggests that XNbs1 BRCT2 could be part of a tandem repeat. This is supported by the conservation of two solvent-exposed hydrophobic residues (Ala239 and Phe242) in the α1 helix of XNbs1 BRCT2, corresponding to Ile2017 and Cys2020 in human MDC1, and Met1783 and Leu1786 in human BRCA1, respectively. These residues in MDC1 and BRCA1 form stabilizing contacts at the inter-BRCT interface. Interestingly, this pattern of exposed hydrophobic residues is also conserved in the first α helix of the monomeric BRCT domain of DNA polymerase μ that is not part of a tandem repeat, suggesting that this α helix could participate in intermolecular interactions with other proteins.[54] Also in support of a packed arrangement of two BRCT domains in Nbs1 is the presence of a 26-residue linker between the end of BRCT1 and the start of BRCT2 in both human and *X. laevis* Nbs1, a feature similar to the 28- and 24-aa linkers that exist in human MDC1 and BRCA1, respectively. A single point R215W mutation in the linker region of human Nbs1—which may affect the packing interaction of the two BRCT domains—has been linked to increased risk of cancer.[55,56] Finally, similar to XNbs1 BRCT2, the second BRCT domain of BRCA1 was also found to be monomeric and well folded even in the absence of the first BRCT domain.[57] A direct demonstration of the presence of tandem BRCT domains in XNbs1 was not possible, as we could not express the putative tandem repeat or the N-terminal BRCT domain (BRCT1) in *E. coli*. An overlay of the NMR structure of XNbs1 BRCT2 to the crystal structure of human MDC1 tandem BRCT domains bound to a histone γH2AX peptide[33] is presented in Fig. 3a. We note that the disordered loop L3 of XNbs1 is on the same side but does not overlap with the phosphopeptide binding site of MDC1.

Since the tandem BRCT domains of MDC1 and BRCA1 bind phosphoserine-containing proteins, it is likely that XNbs1 could also form a complex with a phosphorylated protein target. Figure 1a shows the structure of MDC1 in complex with a histone γH2AX peptide, highlighting the phosphoserine 139 of γH2AX. The residues in MDC1 and BRCA1 that contact the phosphoserine all come from BRCT1, following the patterns of Ser/Thr-Gly in the β1–α1 loop and Ser/Thr-Xxx-Lys in the α2 helix.[58] These amino acid patterns in the first BRCT domain of MDC1 and BRCA1 are well conserved in Nbs1. For the Ser/Thr-Gly pattern, XNbs1 and human Nbs1

have Ser116 and Ser118, respectively, with a cysteine replacing the glycine in both species. For the Ser/Thr-Xxx-Lys pattern, XNbs1 has Thr156 and Lys158 while human Nbs1 has Thr158 and Lys160.

A number of reports have suggested that Nbs1 could directly bind γH2AX.[59,60] However, from structure and amino acid sequence comparison between XNbs1 and MDC1, it is unlikely that Nbs1 tandem BRCT domains would recognize γH2AX in the same manner as MDC1. The recognition of γH2AX by MDC1 is mediated by key interactions involving the last amino acid of histone H2AX, Tyr142. Tyr142 binds at the interface formed by the two BRCT domains of MDC1 and is in close contact with Pro2009 of MDC1 BRCT2, as highlighted in Fig. 3a, while its carboxy group forms an essential salt bridge with the guanidinium group of Arg1933 of MDC1 BRCT1.[33] Based on amino acid alignments, Arg1933 of MDC1 is replaced by Val155 in XNbs1 and Val157 in human Nbs1 (data not shown). From a 3-D structure-based alignment of MDC1 and XNbs1 BRCT2 amino acid sequences, Pro2009 of MDC1, which contacts γH2AX Tyr142, occupies a position close to that of XNbs1 Lys231 (Fig. 3b). Therefore, the typical phosphopeptide motif—an aromatic amino acid (Phe or Tyr142) three residues away (+3) from the phosphoserine (pSer139 of γH2AX)—recognized by MDC1[33] and BRCA1[29] may not apply to Nbs1 tandem BRCT domains. In the case of Nbs1, it is tempting to speculate that an aspartate or a glutamate (instead of Phe or Tyr) at +3 position to pSer would be a more favored residue as it could form a charge or salt bridge interaction with Lys233 of human Nbs1 or Lys231 of XNbs1. It was noted previously that Lys233 of human Nbs1 is acetylated and that this process is tightly regulated by the

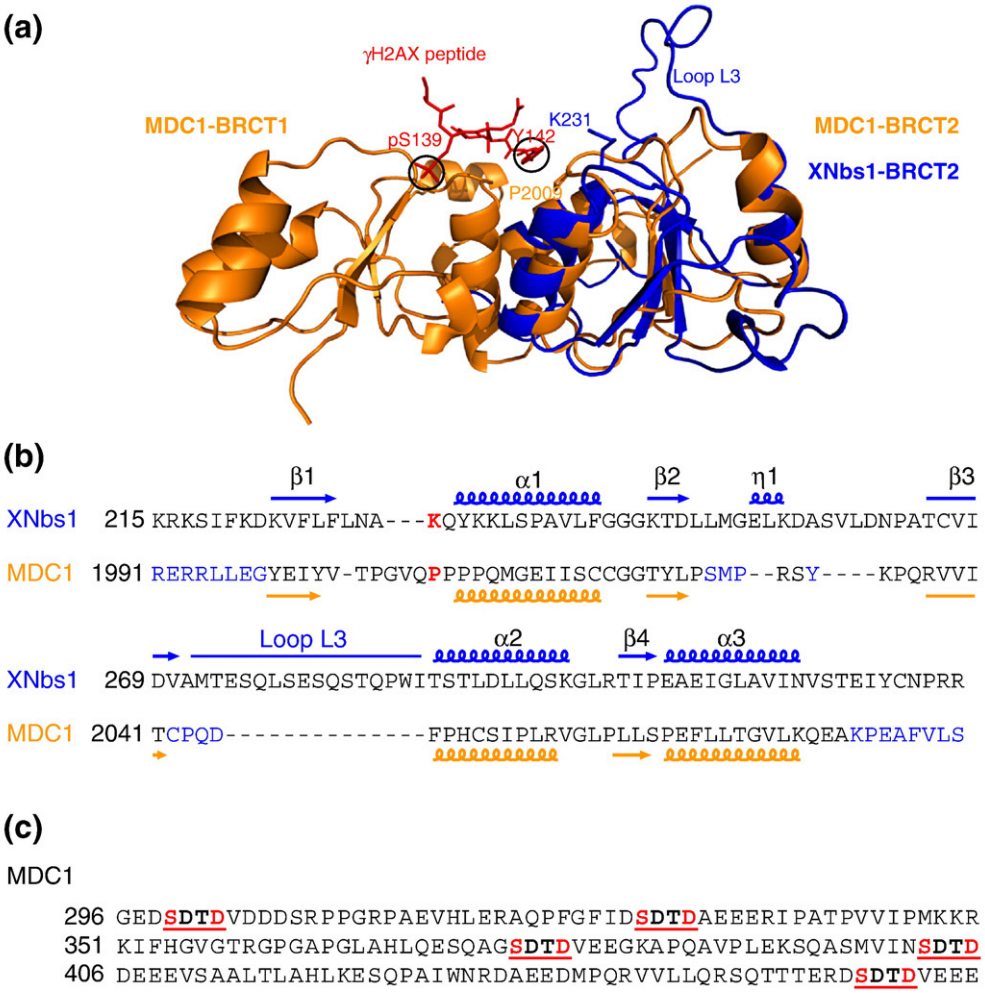

Fig. 3. Structural and functional relationship of Nbs1 and MDC1. (a) The lowest energy NMR structure of XNbs1 (215–324 aa), shown in blue and labeled Nbs1-BRCT2, is superimposed on the second BRCT domain of human MDC1 (MDC1-BRCT2) from the X-ray structure of the complex of MDC1 (orange) and γH2AX (red). The pSer139 and Tyr142 at (pSer +3) position of γH2AX are highlighted. XNbs1 Lys231 and MDC1 Pro2009 that contacts γH2AX Tyr142 are shown. (b) 3-D structure-based alignment of XNbs1 BRCT2 and human MDC1 BRCT2. The secondary-structure elements of XNbs1 and MDC1 are shown in blue and orange, respectively. Residues of MDC1 that do not match the structure of XNbs1 are shown in blue. MDC1 Pro2009 and XNbs1 Lys231 are colored red. (c) Amino acid sequence of human MDC1 with the five SDTD repeats highlighted.

deacetylase SIRT1 as part of the DNA damage response.[40] Acetylation and deacetylation of this lysine may therefore regulate the binding of Nbs1 to its phosphorylated target.

In recent studies, it was shown that a direct interaction between Nbs1 N-terminal FHA domain and phosphorylated MDC1 is necessary for the retention of the MRN complex at DNA damage sites.[61–63] MDC1 is constitutively phosphorylated by casein kinase 2 (CK2) at serine and threonine residues in Ser-Asp-Thr (SDT) repeats. There are five such SDT repeats (from residues 299 to 456) in human MDC1 (Fig. 3c). Remarkably, all five repeats have an aspartate at position pSer +3 (i.e., pSer-Asp-pThr-Asp), what we predicted to be favorable for binding Nbs1 tandem BRCT domains, as the side-chain ammonium group of Nbs1 Lys233 or XNbs1 Lys231 could participate in a charge interaction with the aspartate. This aspartate is conserved in MDC1 from other species (data not shown). Furthermore, the large number of residues separating the MDC1 repeats (Fig. 3c) suggests a possible dual-binding mode with threonine-phosphorylated repeats interacting with the FHA domain of Nbs1 and serine-phosphorylated repeats interacting with the tandem BRCT domains of Nbs1.

BRCT2 is essential for the MDC1-dependent nuclear relocalization of Nbs1 to DNA damage sites

The importance of BRCT2 for the function of human Nbs1 was tested *in vivo* by probing the ability of full-length human Nbs1 to form foci at DNA damage sites. MDC1 is required for Nbs1 foci formation following DNA damage. Early studies have suggested that an interaction between MDC1 and Nbs1 may be responsible for the recruitment of Nbs1 to DNA damage sites,[33,64] and, as mentioned above, recent studies have shown that such interaction is dependent on MDC1 phosphorylation. Indeed, we noticed that co-expression of MDC1 greatly enhanced the accumulation of exogenous Nbs1 to DNA damage foci (Fig. 4a and b). To assess whether mutations within Nbs1 BRCT2 domain would affect Nbs1 foci formation, we used constructs encoding Flag-tagged wild type or BRCT2 mutants of Nbs1. We chose the following human Nbs1 mutations—G247R, V270P, and V271R—based on the NMR structure of XNbs1. The corresponding XNbs1 residues, Gly243, Val267, and Ile268, are all predicted to be essential for the structural integrity of BRCT2. A bulky arginine side chain replacing Gly243, in a loop between α1 and β2, is expected to project into the hydrophobic core of BRCT2 and thus destabilize this domain. The amino acids Val267 and Ile268 are part of the BRCT2 hydrophobic core, and, consequently, their replacement by a proline and an arginine, respectively, is expected to prevent the domain from folding properly.

HeLa cells were transfected with the Nbs1-expressing constructs together with a plasmid encoding MDC1. The foci formation of exogenous Nbs1 was then evaluated by immunostaining following IR (10 Gy). As shown in Fig. 4a and b, while wild-type Nbs1 localized normally to damage-induced foci, all three BRCT2 mutants failed to do so. Together, these data indicate that the second BRCT domain of Nbs1 is important for Nbs1 localization and function following DNA damage.

As we have explained previously, BRCT2 of XNbs1 could be part of a tandem repeat that would bind a phosphorylated protein target. The identification of a lysine residue (Lys231 in XNbs1 and Lys233 in human Nbs1) at a position known to contact the residue +3 to the phosphopeptide bound to BRCA1 and MDC1 tandem BRCT domains, suggest that this lysine could interact with the (pSer +3) aspartate side chain of the CK2-phosphorylated pSer-Asp-pThr-Asp repeats of MDC1. Mutation of Nbs1 Lys233 into an alanine prevented the MDC1-dependent relocalization of Nbs1 to DNA damage-induced foci, while its mutation into an arginine did not markedly affect relocalization (Fig. 4a and b), demonstrating the functional importance of this lysine and the need for a positively charged residue at its position.

Using NMR spectroscopy, we verified that mutation of the corresponding lysine in XNbs1 into an arginine and alanine does not disrupt the BRCT fold. As shown in Fig. 4c, the ^{1}H–^{15}N HSQC spectra of XNbs1 BRCT2 wild type as well as K231A and K231R mutants are virtually identical. The only changes observed in the spectra are for residues in the vicinity of the mutated Lys231. Taken together, these results demonstrate that Lys233 is key to the function of human Nbs1 and strongly suggest that Lys233 contributes to a salt bridge in a protein–protein interaction, most likely the interaction of Nbs1 tandem BRCT domains with phosphorylated MDC1.

Conclusion

We have shown that XNbs1 has a second BRCT domain, conserved in human Nbs1, that most likely forms a tandem repeat with the first BRCT domain. Nbs1 foci formation is closely linked to both the presence of histone γH2AX and MDC1. It is well established that the tandem BRCT domains of MDC1 form a complex with γH2AX. Since a direct interaction of Nbs1 with γH2AX is improbable, as discussed here, it is possible that the putative tandem BRCT domains of Nbs1 bind phosphorylated MDC1. Recent results show that MDC1 is phosphorylated at multiple repeat sequences and that this phosphorylation is necessary for the binding of the MRN complex to damaged chromatin. CK2 phosphorylates Ser and Thr residues at Ser-Asp-Thr-Asp clusters of MDC1. Noticeably, in the pSer-Asp-pThr-Asp sequence the +3 position to pSer is an Asp, which according to our prediction based on the structure of BRCT2 in the context of tandem BRCT domains could form a charge interaction with Lys233 of human Nbs1. We have shown that the results of mutating Lys233 into an alanine and arginine are consistent with its involvement in protein–protein interactions. Therefore, the relocalization of Nbs1 to

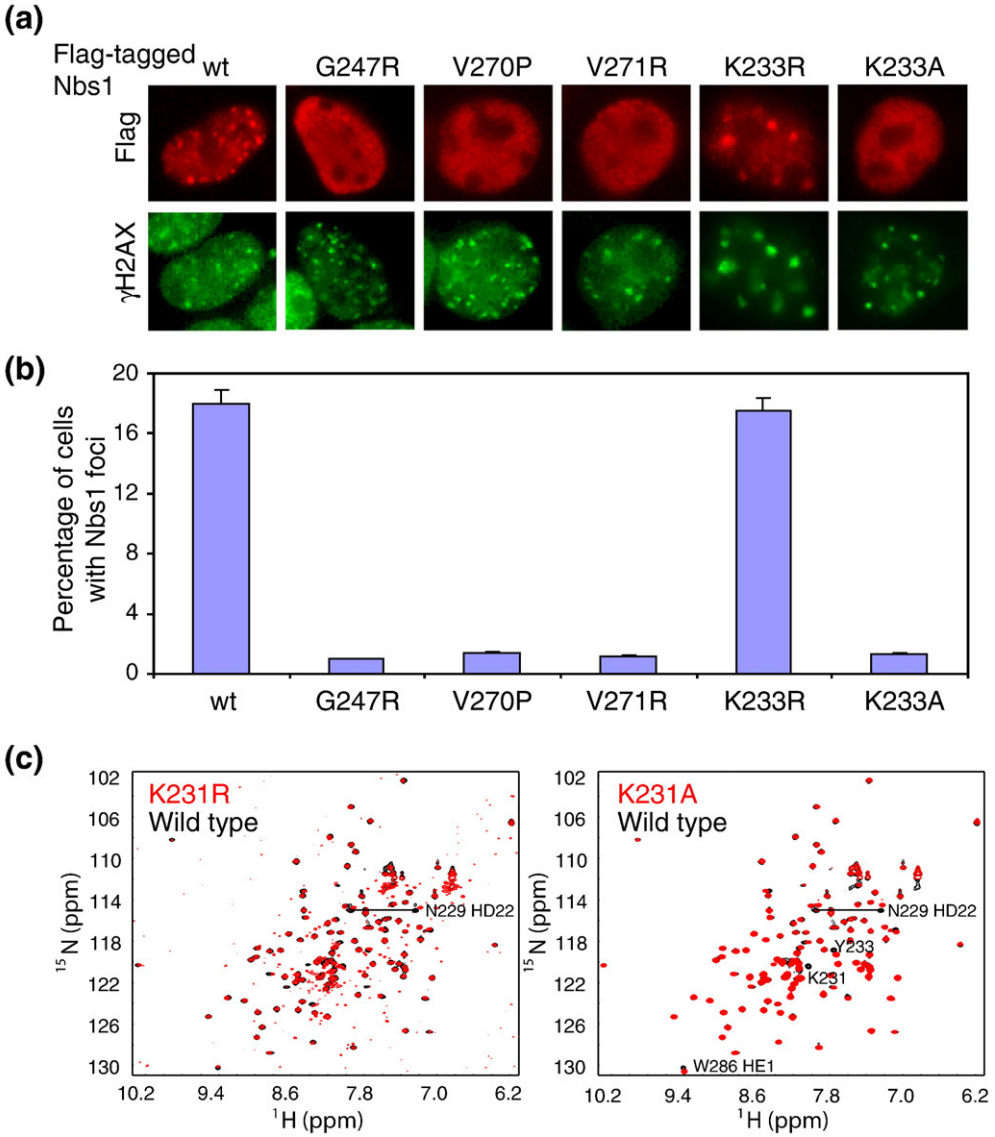

Fig. 4. The BRCT2 domain of human Nbs1 is required for the formation of ionizing-radiation-induced foci. (a) HeLa cells were transfected with plasmids encoding Flag-tagged wild type, G247R, V270P, V271R, K233R, or K233A mutant Nbs1, together with a plasmid encoding HA-tagged human MDC1. Thirty-six hours after transfection, cells were exposed to IR (10 Gy), fixed and immunostained with anti-Flag and anti-γH2AX antibodies. (b) Quantification of Nbs1 foci in cells described in (a). The results are the average of two experiments. (c) Overlay of ^{1}H–^{15}N HSQC spectra of wild-type XNbs1 BRCT2 and K231R and K231A mutants. The spectra of wild-type and mutant proteins are shown in black and red, respectively. Residues displaying a change in chemical shift after mutation of Lys231 are labeled. XNbs1 Lys231 corresponds to Lys233 of human Nbs1.

DNA damage sites may be in part mediated by the direct interaction of Nbs1 tandem BRCT domains with phosphorylated MDC1.

Materials and Methods

Protein production

The DNA corresponding to amino acid residues from 215 to 324 was amplified from *X. laevis* cDNA and cloned in-frame into the NdeI and BamHI sites of a pT7.7 vector. The plasmid was then transformed in competent cells of *E. coli* BL21(DE3) strain. Transformants were used to inoculate LB medium for the production of nonlabeled XNbs1 protein. Cells were grown at 37 °C until an A_{600} of about 0.6 to 0.8 was reached. Next, the culture was transferred to 15 °C where after 45 min it was induced with 1 mM final concentration of IPTG. Incubation was continued for 16 to 20 h after which the cells were harvested.

The following purification steps were all done at 4 °C. Cells were resuspended in 50 mM sodium phosphate, pH 7.5, and 300 mM NaCl (resuspension solution), lyzed with a microfluidizer operating at high pressure (Emulsiflex C5 from Avestin), and then centrifuged. The resulting supernatant fraction was loaded onto a column containing Ni–NTA resin (Qiagen) preequilibrated with the resuspension solution. The column was washed with the resuspension buffer plus 20 mM imidazole. The protein was eluted with a similar buffer containing 500 mM imidazole. Size-exclusion chromatography with Superdex 75 (GE Healthcare)

was performed for the final purification. Protein was >95% pure as judged by SDS-PAGE.

Similar steps were followed for the production of ^{15}N- and $^{15}N/^{13}C$-labeled XNbs1 proteins but using M9 medium (instead of LB medium) containing 1 g/L ^{15}N NH_4Cl and either 4 g/L D-[$^{12}C_6$]glucose and 1 g/L ^{15}N Isogro, or 2 g/L D-[$^{13}C_6$]glucose and 1 g/L $^{15}N/^{13}C$ Isogro (Isotec).

Mutant plasmids (K231R and K231A) of XNbs1 were generated by Quickchange method (Stratagene) and the corresponding proteins were prepared as described above for wild-type XNbs1.

NMR spectroscopy

For NMR experiments, ~0.4 mM of XNbs1 samples were in a buffer containing 20 mM sodium phosphate, pH 6.7, 50 mM NaCl, 50 mM glutamic acid, 50 mM arginine, 2 mM DTT, 1 mM ethylenediaminetetraacetic acid, and 93% H_2O/7% D_2O. All NMR experiments were performed at 15 °C using Bruker Avance 600- and 700-MHz spectrometers equipped with a cryoprobe. NMR data were processed and analyzed with the software NMRPipe/NMRDraw[65] and NMRView.[66]

An ^{15}N-labeled XNbs1 sample was used to collect 2-D ^1H–^{15}N HSQC spectra and ^{15}N-edited NOE spectroscopy (NOESY) spectra with 120 ms mixing time and to measure backbone relaxation parameters: R_1, R_2, and ^1H–^{15}N NOE at two magnetic field strengths (600 and 700 MHz, ^1H frequency). ^{15}N R_1 relaxation rates were measured with 10 different relaxation delays: 10, 35, 80, 120, 170, 240, 350, 500, 720, and 1200 ms, while for ^{15}N R_2 relaxation rates, 14 delays were used: 4, 12, 16, 22, 40, 60, 80, 120, 160, 192, 240, 288, 336, and 400 ms. For both R_1 and R_2 measurements, a recycle delay of 1 s was used. In the measurement of ^1H–^{15}N NOE, spectra were collected with a 2-s relaxation delay followed by a 3-s proton saturation. In the absence of proton saturation, the relaxation delay was extended to 5 s. The reduced spectral density functions were calculated as previously reported.[47,48,50,67]

A double $^{15}N/^{13}C$-labeled sample of XNbs1 was used to collect a series of experiments ^1H–^{13}C HSQC, CBCA(CO)NH, CBCANH, HBHA(CO)NH, HNCO, HN(CA)CO, CCH-correlated spectroscopy (COSY), CCH-total COSY (TOCSY), HCCH-TOCSY, C(CO)NH-TOCSY, H(CCO)NH-TOCSY, and HBCBCGCDHD for backbone and side-chain resonance assignments following well established procedures.[68] In addition, ^{15}N-edited NOESY and ^{13}C-edited NOESY aliphatic and aromatic spectra with a mixing time of 120 ms were also acquired to obtain NOE restraints.

Resonance assignments could not be made for residues Lys215, Arg216, Gln276, Leu277, and Ser278, while the resonances of Lys217, Thr273, Glu274, Gln282, Thr283, and Gln284 were only partially assigned. With the exceptions of Lys215, Arg216, and Lys217, which are at the very N-terminus of XNbs1 BRCT2, all other residues listed above are part of the disordered loop L3.

Structure calculations

Two hundred initial structures of XNbs1 were calculated using a simulated annealing protocol in the program CYANA2.1[69] and experimentally derived proton–proton NOE restraints, calculated dihedral angle restraints generated from CSI[70] and TALOS,[71] and H bonds expected from secondary structures and ultimately confirmed from NOE patterns. The dihedral angles were set to $\phi = -60 \pm 40°$ and $\psi = -50 \pm 40°$ for α helices and $\phi = -139 \pm 40°$ and $\psi = 135 \pm 40°$ for β strands. Hydrogen bonds were defined as H–O and N–O distances of 2 and 3 Å, respectively. Hydrogen bonds were determined in a conservative manner based on the well-defined secondary-structure elements validated by NOEs and were only included at the last stage of structure calculations. $^1H/^2H$ exchange experiments could not be done, as the protein could not be readily resolubilized in D_2O after lyophilization. The structures were refined with AMBER 8[72] following a previously published calculation protocol[67,73] using the generalized Born model to mimic solvent,[74] and producing the final 20 structures with the lowest energies, none of which have distance and angle violations greater than 0.3 Å and 5°, respectively. The list of NMR restraints and statistics of the calculations are summarized in Table 1. Molecular representations were generated using PyMol† and MOLMOL.[75]

Plasmids and transfection procedures for *in vivo* assays

Human MDC1 cDNA was cloned into a pcDNA vector containing HA tag, while human Nbs1 cDNA was cloned into a pIRES2 vector with an N-terminal Flag tag. Nbs1 mutant plasmids (G247R, V270P, V271R, K233A, and K233R) were generated by PCR-based mutagenesis.

HeLa cells were purchased from American Type Culture Collections and maintained in RPMI media supplemented with 10% fetal bovine serum. Transfections were performed using Lipofectamine 2000 reagent (Invitrogen) following the manufacturer's instructions.

Immunofluorescence staining

Thirty-six hours after transfection, HeLa cells were exposed to 10 Gy of IR and then fixed on coverslips with 3% (v/v) paraformaldehyde solution in phosphate-buffered saline (PBS) containing 50 mM sucrose for a period of 10 min at room temperature.

The cells were then permeabilized with 20 mM Hepes, pH 7.4, 50 mM NaCl, 3 mM $MgCl_2$, 300 mM sucrose, and 0.5% (v/v) Triton X-100 at room temperature for 5 min. Next, the cells were washed three times with PBS and then incubated with Flag antibody (Sigma) and γH2AX antibody at 37 °C for 20 min. After another wash with PBS, cells were incubated with fluorescein isothiocyanate or rhodamine-conjugated secondary antibodies at 37 °C for 20 min. Nuclei were counterstained with 4′6-diamidino-2-phenylindole. After a final wash with PBS, the coverslips were mounted on slides with glycerin containing paraphenylenediamine. Cells with and without Nbs1 and γ-H2AX/MDC1 foci were counted under a microscope.

Protein Data Bank accession codes

The atomic coordinates and NMR constraints of XNbs1 BRCT2 have been deposited at the Protein Data Bank under accession code 2K2W.

Acknowledgements

We thank Drs. Tony Hunter and Paul Russell for the gift of *X. laevis* Nbs1 cDNA and Dr. Eva Lee for

† http://pymol.sourceforge.net/

human Nbs1 cDNA. We are grateful to Drs. Slobodan Macura, Nenad Juranic, and Prasanna Mishra at the Mayo NMR core facility for assistance, and Dr. Emeric Wasielewski for helping with the figures. This work was supported by National Institutes of Health grants CA092312 to J.C. and CA109449 to G.M.

References

1. Weemaes, C. M., Hustinx, T. W., Scheres, J. M., van Munster, P. J., Bakkeren, J. A. & Taalman, R. D. (1981). A new chromosomal instability disorder: the Nijmegen breakage syndrome. *Acta Paediatr. Scand.* **70**, 557–564.
2. van der Burgt, I., Chrzanowska, K. H., Smeets, D. & Weemaes, C. (1996). Nijmegen breakage syndrome. *J. Med. Genet.* **33**, 153–156.
3. Shiloh, Y. (1997). Ataxia–telangiectasia and the Nijmegen breakage syndrome: related disorders but genes apart. *Annu. Rev. Genet.* **31**, 635–662.
4. Jongmans, W., Vuillaume, M., Chrzanowska, K., Smeets, D., Sperling, K. & Hall, J. (1997). Nijmegen breakage syndrome cells fail to induce the p53-mediated DNA damage response following exposure to ionizing radiation. *Mol. Cell. Biol.* **17**, 5016–5022.
5. Matsuura, K., Balmukhanov, T., Tauchi, H., Weemaes, C., Smeets, D., Chrzanowska, K. *et al.* (1998). Radiation induction of p53 in cells from Nijmegen breakage syndrome is defective but not similar to ataxia–telangiectasia. *Biochem. Biophys. Res. Commun.* **242**, 602–607.
6. Ito, A., Tauchi, H., Kobayashi, J., Morishima, K., Nakamura, A., Hirokawa, Y. *et al.* (1999). Expression of full-length NBS1 protein restores normal radiation responses in cells from Nijmegen breakage syndrome patients. *Biochem. Biophys. Res. Commun.* **265**, 716–721.
7. Tauchi, H., Matsuura, S., Kobayashi, J., Sakamoto, S. & Komatsu, K. (2002). Nijmegen breakage syndrome gene, NBS1, and molecular links to factors for genome stability. *Oncogene*, **21**, 8967–8980.
8. Matsuura, S., Tauchi, H., Nakamura, A., Kondo, N., Sakamoto, S., Endo, S. *et al.* (1998). Positional cloning of the gene for Nijmegen breakage syndrome. *Nat. Genet.* **19**, 179–181.
9. Varon, R., Vissinga, C., Platzer, M., Cerosaletti, K. M., Chrzanowska, K. H., Saar, K. *et al.* (1998). Nibrin, a novel DNA double-strand break repair protein, is mutated in Nijmegen breakage syndrome. *Cell*, **93**, 467–476.
10. Trujillo, K. M., Yuan, S. S., Lee, E. Y. & Sung, P. (1998). Nuclease activities in a complex of human recombination and DNA repair factors Rad50, Mre11, and p95. *J. Biol. Chem.* **273**, 21447–21450.
11. Carney, J. P., Maser, R. S., Olivares, H., Davis, E. M., Le Beau, M., Yates, J. R., 3rd *et al.* (1998). The hMre11/hRad50 protein complex and Nijmegen breakage syndrome: linkage of double-strand break repair to the cellular DNA damage response. *Cell*, **93**, 477–486.
12. Zhao, S., Renthal, W. & Lee, E. Y. (2002). Functional analysis of FHA and BRCT domains of NBS1 in chromatin association and DNA damage responses. *Nucleic Acids Res.* **30**, 4815–4822.
13. Stracker, T. H., Theunissen, J. W., Morales, M. & Petrini, J. H. (2004). The Mre11 complex and the metabolism of chromosome breaks: the importance of communicating and holding things together. *DNA Repair (Amsterdam)*, **3**, 845–854.
14. van den Bosch, M., Bree, R. T. & Lowndes, N. F. (2003). The MRN complex: coordinating and mediating the response to broken chromosomes. *EMBO Rep.* **4**, 844–849.
15. Petrini, J. H. & Stracker, T. H. (2003). The cellular response to DNA double-strand breaks: defining the sensors and mediators. *Trends Cell Biol.* **13**, 458–462.
16. Paull, T. T. & Gellert, M. (1999). Nbs1 potentiates ATP-driven DNA unwinding and endonuclease cleavage by the Mre11/Rad50 complex. *Genes Dev.* **13**, 1276–1288.
17. Lee, J. H., Ghirlando, R., Bhaskara, V., Hoffmeyer, M. R., Gu, J. & Paull, T. T. (2003). Regulation of Mre11/Rad50 by Nbs1: effects on nucleotide-dependent DNA binding and association with ataxia–telangiectasia-like disorder mutant complexes. *J. Biol. Chem.* **278**, 45171–45181.
18. Desai-Mehta, A., Cerosaletti, K. M. & Concannon, P. (2001). Distinct functional domains of nibrin mediate Mre11 binding, focus formation, and nuclear localization. *Mol. Cell. Biol.* **21**, 2184–2191.
19. Lee, J. H. & Paull, T. T. (2005). ATM activation by DNA double-strand breaks through the Mre11–Rad50–Nbs1 complex. *Science*, **308**, 551–554.
20. Difilippantonio, S., Celeste, A., Fernandez-Capetillo, O., Chen, H. T., Reina San Martin, B., Van Laethem, F. *et al.* (2005). Role of Nbs1 in the activation of the ATM kinase revealed in humanized mouse models. *Nat. Cell Biol.* **7**, 675–685.
21. Cerosaletti, K., Wright, J. & Concannon, P. (2006). Active role for nibrin in the kinetics of ATM activation. *Mol. Cell. Biol.* **26**, 1691–1699.
22. Maser, R. S., Zinkel, R. & Petrini, J. H. (2001). An alternative mode of translation permits production of a variant NBS1 protein from the common Nijmegen breakage syndrome allele. *Nat. Genet.* **27**, 417–421.
23. Featherstone, C. & Jackson, S. P. (1998). DNA repair: the Nijmegen breakage syndrome protein. *Curr. Biol.* **8**, R622–R625.
24. Callebaut, I. & Mornon, J. P. (1997). From BRCA1 to RAP1: a widespread BRCT module closely associated with DNA repair. *FEBS Lett.* **400**, 25–30.
25. Bork, P., Hofmann, K., Bucher, P., Neuwald, A. F., Altschul, S. F. & Koonin, E. V. (1997). A superfamily of conserved domains in DNA damage-responsive cell cycle checkpoint proteins. *FASEB J.* **11**, 68–76.
26. Durocher, D., Smerdon, S. J., Yaffe, M. B. & Jackson, S. P. (2000). The FHA domain in DNA repair and checkpoint signaling. *Cold Spring Harbor Symp. Quant. Biol.* **65**, 423–431.
27. Manke, I. A., Lowery, D. M., Nguyen, A. & Yaffe, M. B. (2003). BRCT repeats as phosphopeptide-binding modules involved in protein targeting. *Science*, **302**, 636–639.
28. Yu, X., Chini, C. C., He, M., Mer, G. & Chen, J. (2003). The BRCT domain is a phospho-protein binding domain. *Science*, **302**, 639–642.
29. Botuyan, M. V., Nomine, Y., Yu, X., Juranic, N., Macura, S., Chen, J. & Mer, G. (2004). Structural basis of BACH1 phosphopeptide recognition by BRCA1 tandem BRCT domains. *Structure*, **12**, 1137–1146.
30. Clapperton, J. A., Manke, I. A., Lowery, D. M., Ho, T., Haire, L. F., Yaffe, M. B. & Smerdon, S. J. (2004). Structure and mechanism of BRCA1 BRCT domain recognition of phosphorylated BACH1 with implications for cancer. *Nat. Struct. Mol. Biol.* **11**, 512–518.
31. Shiozaki, E. N., Gu, L., Yan, N. & Shi, Y. (2004). Structure of the BRCT repeats of BRCA1 bound to a BACH1 phosphopeptide: implications for signaling. *Mol. Cell*, **14**, 405–412.
32. Williams, R. S., Lee, M. S., Hau, D. D. & Glover, J. N. (2004). Structural basis of phosphopeptide recognition by the BRCT domain of BRCA1. *Nat. Struct. Mol. Biol.* **11**, 519–525.

33. Stucki, M., Clapperton, J. A., Mohammad, D., Yaffe, M. B., Smerdon, S. J. & Jackson, S. P. (2005). MDC1 directly binds phosphorylated histone H2AX to regulate cellular responses to DNA double-strand breaks. *Cell*, **123**, 1213–1226.
34. Lee, M. S., Edwards, R. A., Thede, G. L. & Glover, J. N. (2005). Structure of the BRCT repeat domain of MDC1 and its specificity for the free COOH-terminal end of the gamma-H2AX histone tail. *J. Biol. Chem.* **280**, 32053–32056.
35. Falck, J., Coates, J. & Jackson, S. P. (2005). Conserved modes of recruitment of ATM, ATR and DNA-PKCs to sites of DNA damage. *Nature*, **434**, 605–611.
36. You, Z., Chahwan, C., Bailis, J., Hunter, T. & Russell, P. (2005). ATM activation and its recruitment to damaged DNA require binding to the C terminus of Nbs1. *Mol. Cell. Biol.* **25**, 5363–5379.
37. Gatei, M., Young, D., Cerosaletti, K. M., Desai-Mehta, A., Spring, K., Kozlov, S. *et al.* (2000). ATM-dependent phosphorylation of nibrin in response to radiation exposure. *Nat. Genet.* **25**, 115–119.
38. Lim, D. S., Kim, S. T., Xu, B., Maser, R. S., Lin, J., Petrini, J. H. & Kastan, M. B. (2000). ATM phosphorylates p95/Nbs1 in an S-phase checkpoint pathway. *Nature*, **404**, 613–617.
39. Lee, J. H., Xu, B., Lee, C. H., Ahn, J. Y., Song, M. S., Lee, H. *et al.* (2003). Distinct functions of Nijmegen breakage syndrome in ataxia telangiectasia mutated-dependent responses to DNA damage. *Mol. Cancer Res.* **1**, 674–681.
40. Yuan, Z., Zhang, X., Sengupta, N., Lane, W. S. & Seto, E. (2007). SIRT1 regulates the function of the Nijmegen breakage syndrome protein. *Mol. Cell.* **27**, 149–162.
41. Becker, E., Meyer, V., Madaoui, H. & Guerois, R. (2006). Detection of a tandem BRCT in Nbs1 and Xrs2 with functional implications in the DNA damage response. *Bioinformatics*, **22**, 1289–1292.
42. Romero, P., Obradovic, Z., Li, X., Garner, E. C., Brown, C. J. & Dunker, A. K. (2001). Sequence complexity of disordered protein. *Proteins*, **42**, 38–48.
43. Laskowski, R. A., Rullmannn, J. A., MacArthur, M. W., Kaptein, R. & Thornton, J. M. (1996). AQUA and PROCHECK-NMR: programs for checking the quality of protein structures solved by NMR. *J. Biomol. NMR*, **8**, 477–486.
44. Ishima, R., Yamasaki, K., Saito, M. & Nagayama, K. (1995). Spectral densities of nitrogen nuclei in *Escherichia coli* ribonuclease HI obtained by ^{15}N NMR relaxation and molecular dynamics. *J. Biomol. NMR*, **6**, 217–220.
45. Peng, J. W. & Wagner, G. (1995). Frequency spectrum of NH bonds in eglin c from spectral density mapping at multiple fields. *Biochemistry*, **34**, 16733–16752.
46. Farrow, N. A., Zhang, O., Szabo, A., Torchia, D. A. & Kay, L. E. (1995). Spectral density function mapping using ^{15}N relaxation data exclusively. *J. Biomol. NMR*, **6**, 153–162.
47. Mer, G., Dejaegere, A., Stote, R., Kieffer, B. & Lefèvre, J. F. (1996). Structural dynamics of PMP-D2: an experimental and theoretical study. *J. Phys. Chem.* **100**, 2667–2674.
48. Lefèvre, J. F., Dayie, K. T., Peng, J. W. & Wagner, G. (1996). Internal mobility in the partially folded DNA binding and dimerization domains of GAL4: NMR analysis of the N–H spectral density functions. *Biochemistry*, **35**, 2674–2686.
49. Abragam, A. (1961). *The Principles of Nuclear Magnetism.* Clarendon Press, Oxford, UK.
50. Atkinson, R. A. & Kieffer, B. (2004). The role of protein motions in molecular recognition: insights from heteronuclear NMR relaxation measurements. *Prog. Nucl. Magn. Reson. Spectrosc.* **44**, 141–187.
51. Stewart, G. S., Last, J. I., Stankovic, T., Haites, N., Kidd, A. M., Byrd, P. J. & Taylor, A. M. (2001). Residual ataxia telangiectasia mutated protein function in cells from ataxia telangiectasia patients, with 5762ins137 and 7271T→G mutations, showing a less severe phenotype. *J. Biol. Chem.* **276**, 30133–30141.
52. Kim, S. T., Xu, B. & Kastan, M. B. (2002). Involvement of the cohesin protein, Smc1, in ATM-dependent and independent responses to DNA damage. *Genes Dev.* **16**, 560–570.
53. Holm, L. & Sander, C. (1996). Mapping the protein universe. *Science*, **273**, 595–603.
54. DeRose, E. F., Clarkson, M. W., Gilmore, S. A., Galban, C. J., Tripathy, A., Havener, J. M. *et al.* (2007). Solution structure of polymerase μ's BRCT domain reveals an element essential for its role in nonhomologous end joining. *Biochemistry*, **46**, 12100–12110.
55. Varon, R., Reis, A., Henze, G., von Einsiedel, H. G., Sperling, K. & Seeger, K. (2001). Mutations in the Nijmegen breakage syndrome gene (NBS1) in childhood acute lymphoblastic leukemia (ALL). *Cancer Res.* **61**, 3570–3572.
56. Steffen, J., Varon, R., Mosor, M., Maneva, G., Maurer, M., Stumm, M. *et al.* (2004). Increased cancer risk of heterozygotes with NBS1 germline mutations in Poland. *Int. J. Cancer*, **111**, 67–71.
57. Gaiser, O. J., Ball, L. J., Schmieder, P., Leitner, D., Strauss, H., Wahl, M. *et al.* (2004). Solution structure, backbone dynamics, and association behavior of the C-terminal BRCT domain from the breast cancer-associated protein BRCA1. *Biochemistry*, **43**, 15983–15995.
58. Glover, J. N., Williams, R. S. & Lee, M. S. (2004). Interactions between BRCT repeats and phosphoproteins: tangled up in two. *Trends Biochem. Sci.* **29**, 579–585.
59. Kobayashi, J., Tauchi, H., Sakamoto, S., Nakamura, A., Morishima, K., Matsuura, S. *et al.* (2002). NBS1 localizes to γ-H2AX foci through interaction with the FHA/BRCT domain. *Curr. Biol.* **12**, 1846–1851.
60. di Masi, A., Viganotti, M., Polticelli, F., Ascenzi, P., Tanzarella, C. & Antoccia, A. (2008). The R215W mutation in NBS1 impairs γ-H2AX binding and affects DNA repair: molecular bases for the severe phenotype of 657del5/R215W Nijmegen breakage syndrome patients. *Biochem. Biophys. Res. Commun.* **369**, 835–840.
61. Melander, F., Bekker-Jensen, S., Falck, J., Bartek, J., Mailand, N. & Lukas, J. (2008). Phosphorylation of SDT repeats in the MDC1 N terminus triggers retention of NBS1 at the DNA damage-modified chromatin. *J. Cell Biol.* **181**, 213–226.
62. Spycher, C., Miller, E. S., Townsend, K., Pavic, L., Morrice, N. A., Janscak, P. *et al.* (2008). Constitutive phosphorylation of MDC1 physically links the MRE11–RAD50–NBS1 complex to damaged chromatin. *J. Cell Biol.* **181**, 227–240.
63. Wu, L., Luo, K., Lou, Z. & Chen, J. (In press). MDC1 regulates intra-S phase checkpoint by targeting NBS1 to DNA double-strand breaks. *Proc. Natl Acad. Sci. USA.*
64. Lukas, C., Melander, F., Stucki, M., Falck, J., Bekker-Jensen, S., Goldberg, M. *et al.* (2004). Mdc1 couples DNA double-strand break recognition by Nbs1 with its H2AX-dependent chromatin retention. *EMBO J.* **23**, 2674–2683.
65. Delaglio, F., Grzesiek, S., Vuister, G. W., Zhu, G., Pfeifer, J. & Bax, A. (1995). NMRPipe: a multidimensional spectral processing system based on UNIX pipes. *J. Biomol. NMR*, **6**, 277–293.

66. Johnson, B. A. & Blevins, R. A. (1994). NMRView: a computer program for visualization and analysis of NMR data. *J. Biomol. NMR*, **4**, 603–614.
67. Botuyan, M. V., Mer, G., Yi, G. S., Koth, C. M., Case, D. A., Edwards, A. M. *et al.* (2001). Solution structure and dynamics of yeast elongin C in complex with a von Hippel–Lindau peptide. *J. Mol. Biol.* **312**, 177–186.
68. Ferentz, A. E. & Wagner, G. (2000). NMR spectroscopy: a multifaceted approach to macromolecular structure. *Q. Rev. Biophys.* **33**, 29–65.
69. Herrmann, T., Güntert, P. & Wüthrich, K. (2002). Protein NMR structure determination with automated NOE assignment using the new software CANDID and the torsion angle dynamics algorithm DYANA. *J. Mol. Biol.* **319**, 209–227.
70. Wishart, D. S. & Sykes, B. D. (1994). The ^{13}C chemical-shift index: a simple method for the identification of protein secondary structure using ^{13}C chemical-shift data. *J. Biomol. NMR*, **4**, 171–180.
71. Cornilescu, G., Delaglio, F. & Bax, A. (1999). Protein backbone angle restraints from searching a database for chemical shift and sequence homology. *J. Biomol. NMR*, **13**, 289–302.
72. Case, D. A., Darde, T. A., Cheatham, T. E., III, Simmerling, C. L., Wang, J., Duke, R. E. *et al.* (2004). AMBER 8, University of California, San Francisco, CA.
73. Mer, G., Bochkarev, A., Gupta, R., Bochkareva, E., Frappier, L., Ingles, C. J. *et al.* (2000). Structural basis for the recognition of DNA repair proteins UNG2, XPA, and RAD52 by replication factor RPA. *Cell*, **103**, 449–456.
74. Bashford, D. & Case, D. A. (2000). Generalized Born models of macromolecular solvation effects. *Annu. Rev. Phys. Chem.* **51**, 129–152.
75. Koradi, R., Billeter, M. & Wuthrich, K. (1996). MOLMOL: a program for display and analysis of macromolecular structures. *J. Mol. Graphics*, **14**, 51–55, 29–32.